Symmetry properties of Raman heterodyne signals in Pr^{3+}:LaF_3

Y. Takahashi, K. Ishikawa, Y. Fukuda, T. Yabuzaki, and T. Hashi
Department of Physics, Faculty of Science, Kyoto University, Kyoto 606, Japan
(Received 23 February 1990)

We have observed various symmetry properties of the Raman heterodyne signals of spin echoes of ^{141}Pr nuclei in Pr^{3+}:LaF_3 and explained them. We have theoretically derived a general symmetry law that governs the symmetry property of the signals for the static magnetic-field reversal. Observed symmetry properties could be explained by using this law and the nature of the product of three matrix elements relevant to the Raman heterodyne process. In some cases the symmetry properties could be explained only from a consideration of the geometrical symmetry of the system. Numerical calculations were performed under some assumptions on the optical pumping and the effect of level multiplicity, and the results qualitatively support the explanation of observed symmetry properties. Several symmetry properties that have not been observed are predicted.

I. INTRODUCTION

Raman heterodyne detection (RHD) of magnetic resonance[1] has been widely used in solids and gases[2–8] because of its high sensitivity and phase-sensitive characteristics. However, the behavior of the Raman heterodyne signal (RHS) in solids (for example, Pr^{3+}:LaF_3) is far from being completely understood and apparently anomalous behaviors have been observed.[4,5] From the anomalous path dependence of RHS in Pr^{3+}:LaF_3 we found evidence confirming the twinning of the LaF_3 crystal.[5]

The examination of symmetry properties of RHS is one of the most important and fundamental problems. Mitsunaga *et al.*[2] observed that the RHS for the transition $I_z=\pm\frac{5}{2}\leftrightarrow\pm\frac{3}{2}$ (16-MHz signal) inverts its sign for the magnetic field reversal but that for $I_z=\pm\frac{3}{2}\leftrightarrow\pm\frac{1}{2}$ (8-MHz signal) does not. This is one of the important symmetry properties but no explanation has been given.

In this paper we report on the observation of various symmetry properties of RHS in Pr^{3+}:LaF_3 in a static magnetic field (~ 100 Oe) and their explanation. The interference of the RHS from different sites was examined,[2,3] but, to our knowledge, the detailed examination of symmetry properties for a single-site ion in a static magnetic field in Pr^{3+}:LaF_3 has not been reported.

We observed RHS of spin echoes in Pr^{3+}:LaF_3 and examined their symmetry properties in detail. Some of them could be explained by using only the geometrical symmetry of the system. Others could be explained by using a general symmetry law of RHS for the magnetic field reversal, which we have derived theoretically. This law indicates that if the product of three matrix elements relevant to the Raman heterodyne process is real (or pure imaginary), the RHS changes (or does not change) its sign for the magnetic field reversal. The observed symmetry properties including the difference of symmetries for the 16- and 8-MHz transitions could be explained by using this law and the nature of the product. Numerical calculations were also performed to confirm the qualitative explanation of the observed symmetry properties.

In Sec. II we describe the outline of the experiment and the observed symmetry properties of RHS. In Sec. III and an appendix the expression of RHS for a three-level system in a static magnetic field is derived. In Sec. IV we give the geometrical explanation of some symmetry properties. In Sec. V we derive the general symmetry law for the RHS using the expression of RHS and the property of the rotation matrix $D^{(5/2)}_{j,k}(\alpha,\beta,\gamma)$.[9,10] By using this law and transition diagrams, we explain the different symmetry properties of the 16- and 8-MHz signals in Sec. VI. In Sec. VII the results of the numerical calculations are presented and compared to the observation. The effects of optical pumping and multiplicity of the levels are discussed. In Sec. VIII we predict the symmetry properties of the RHS which have not been observed.

II. OBSERVATION OF SYMMETRY PROPERTIES

We observed RHS of spin echoes of ^{141}Pr ($I=\frac{5}{2}$) in the ground-state sublevels of Pr^{3+}:LaF_3. The experimental setup and procedure are essentially the same as those in Ref. 5. As shown in Fig. 1 the sample crystal (0.1 mol %) at 2K is irradiated with a linearly polarized light propa-

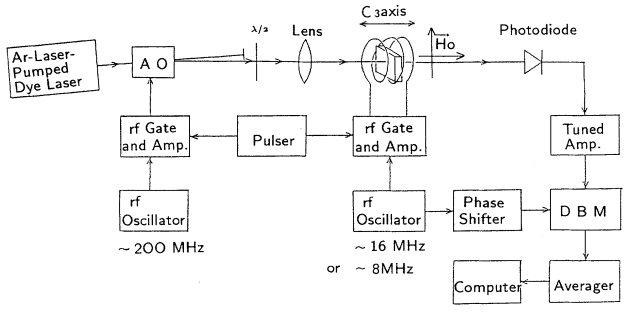

FIG. 1. Experimental setup. AO is an acousto-optic modulator and DBM is a double balanced mixer.

gating along the C_3 axis from a dye laser tuned to the $^3H_4$-$^1D_2$ transition. The laser beam diameter at the sample is about 300 μm. In order to simplify the experimental condition, the light beam is gated, which is different from the procedure in Refs. 1 and 2. As shown in Fig. 2(a) a pump light pulse ($\sim$50 ms, $\sim$10 mW) is applied to create population differences between ground-state sublevels with optical pumping. After a time much longer than the radiative lifetime ($\sim$0.5 ms) of the optical transition, rf pulses are applied to generate spin echoes in the ground state. The rf field is parallel to the C_3 axis. A static magnetic field $\mathbf{H}_0$ of about 100 Oe is applied perpendicular or parallel to the C_3 axis. A probe light pulse ($\sim$10 mW) is applied at the echo time, and the signals are detected as heterodyne beats of the induced Raman and the probe lights. The phase of the reference rf signal is adjusted so that the maximum bell-shaped echo signal is obtained. There are six magnetically inequivalent sites of Pr ions in the crystal.[11] We separately detected signals for these sites by choosing rf frequency, the polarization of the laser beam, and the path of the laser beam through the crystal.[5] The laser frequency is swept to avoid the decrease of signal intensity due to the optical pumping. The sweep rate is so small that the laser frequency remains within the jitter ($\sim$3 MHz) during the single shot.

The observed symmetry properties are shown in Table I. In this table "Odd" means that the sign of the signal is inverted (or its phase is shifted by 180°) for the operations indicated, whereas "Even" means that the signal is unchanged. The symmetry properties indicated by an aster-

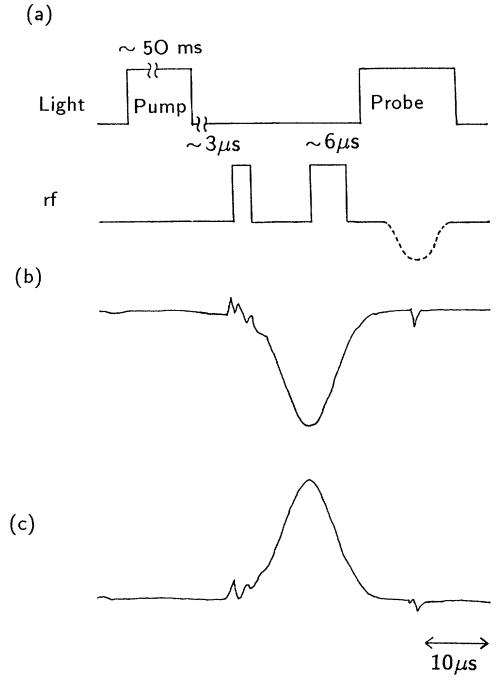

FIG. 2. (a) Pulse sequence. (b) and (c) typical spin echo signals under normal (b) and reversed (c) field conditions, respectively, to illustrate the basis for Table I as well as the quality of signals which permitted the categorical assignments in the table.

TABLE I. Observed symmetry properties in the case of $\mathbf{H}_1 \| \mathbf{C}_3$. "Odd" means that the sign of the signal is inverted for the operations indicated, whereas "Even" means that the signal is unchanged. This notation is the same as that in Ref. 2.

	(1)		(2)		(3)		(4)
rf transition	field reversal $\vec{H}_o \longleftrightarrow -\vec{H}_o$		site interchange *Asite* $\longleftrightarrow$ *Bsite*		Zeeman spectra $\xi \longleftrightarrow \eta$		$\theta \equiv \angle(\vec{H}_o, \vec{C}_2)$ $\theta \longleftrightarrow -\theta$
	$\vec{H}_o \perp \vec{C}_3^*$	$\vec{H}_o \parallel \vec{C}_3$	$\vec{H}_o \perp \vec{C}_3$	$\vec{H}_o \parallel \vec{C}_3$	$\vec{H}_o \perp \vec{C}_3^*$	$\vec{H}_o \parallel \vec{C}_3^{\#}$	$\vec{H}_o \perp \vec{C}_3^*$
$\pm\frac{3}{2} \leftrightarrow \pm\frac{5}{2}$ ($\sim 16MHz$)	odd	odd	odd	even	odd	odd	odd
$\pm\frac{1}{2} \leftrightarrow \pm\frac{3}{2}$ ($\sim 8MHz$)	even	odd	even	even	even	odd	odd
	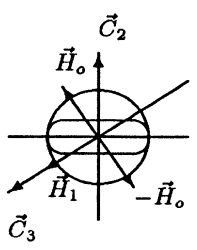		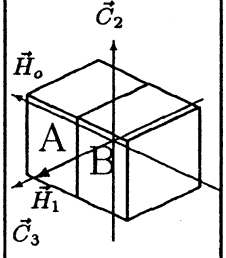		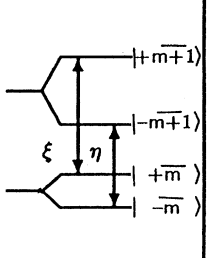		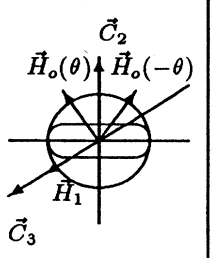

isk were examined previously[2] by the cw method and the results are the same as ours. The property indicated by # is an expectation and has not been observed. There are two kinds of transitions $I_z=\pm\frac{5}{2}\leftrightarrow\pm\frac{3}{2}$ ($\sim$16 MHz) and $I_z=\pm\frac{3}{2}\leftrightarrow\pm\frac{1}{2}$ ($\sim$8 MHz) in the ground state. The symmetry properties are generally different for these transitions. The first column shows the symmetry properties (1) for the magnetic field reversal. As shown in Ref. 5 there are A and B sites relating to the crystal twinning of LaF_3. These sites are interchanged by 180° rotation about the C_3 axis. The second column shows the properties (2) of the signals for the interchange of these sites. The third column shows the properties (3) of the signals when the transitions $|\overline{m}\rangle\leftrightarrow|(m+1)\rangle$ and $|-\overline{m}\rangle\leftrightarrow|-(m+1)\rangle$ are interchanged by changing the rf frequency. The fourth column shows the properties (4) of the signals when the direction of the magnetic field $\mathbf{H}_0$ is changed in the plane perpendicular to the C_3 axis as shown in the attached figure. These symmetry properties are very complicated and no explanation has been given so far.

In Figs. 2(b) and 2(c) typical spin echo signals are shown under normal (b) and reversed (c) field conditions, respectively, to illustrate the basis for Table I as well as the quality of signals which permitted the categorical assignments in the table.

We classify these symmetry properties into two groups. The first group is the one that can be interpreted simply by using the geometrical symmetry. The symmetry properties (1), (2), and (3) for $\mathbf{H}_0\|\mathbf{C}_3$, and (4) belong to the first group. The interpretation is given in Sec. IV.

The rest of the symmetry properties, that is, properties (1), (2), and (3) for $\mathbf{H}_0\perp\mathbf{C}_3$ belong to the second group which cannot be interpreted only by geometrical symmetry. It can easily be shown that the symmetry property (3) is a direct consequence of (1). Moreover, since A and B sites are interchanged by 180° rotation about the C_3 axis,[5] property (2) can be derived from (1); the direction of $\mathbf{H}_0$ is inverted by the interchange of A and B sites when $\mathbf{H}_0\perp\mathbf{C}_3$. Therefore in order to explain the symmetry properties belonging to the second group, it is enough for us to explain one of them. We take up the symmetry property (1) for $\mathbf{H}_0\perp\mathbf{C}_3$. The explanation is given in Secs. VI and VII.

III. EXPRESSION OF RHS FOR A THREE-LEVEL SYSTEM

Figure 3 shows relevant energy levels of Pr^{3+}:LaF_3.[11] Both the ground and excited states are electronic singlets, but each of them splits into three Kramers doublets by the electric quadrupole interaction. Application of a weak magnetic field lifts the twofold degeneracy and results in the energy levels as shown. Both the ground and excited states are subjected to nonaxial quadrupole interactions whose principal axes do not coincide with each other[2,11] as shown in Fig. 4.

We take up a three-level system as shown in Fig. 5. The levels $|1\rangle$ and $|2\rangle$ are two of the ground-state sublevels between which magnetic dipole transition is allowed and $|3\rangle$ is one of the optically excited states. Electric dipole transitions are allowed between $|1\rangle$ and $|3\rangle$ and between $|2\rangle$ and $|3\rangle$. $\omega_{ij}/2\pi$ indicates the frequency splitting between the levels $|i\rangle$ and $|j\rangle$ ($i,j=1,2$, and 3). $\omega_E/2\pi$ and $\omega_H/2\pi$ are the frequencies of the probe laser and the rf magnetic field. The detunings Δ and Δ_H are $\omega_{32}-\omega_E$ and $\omega_{21}-\omega_H$, respectively. We neglect the inhomogeneous broadening of the $|1\rangle$-$|2\rangle$ transition, and treat the case of just resonance for the rf transition ($\omega_H=\omega_{21}$, $\Delta_H=0$). We also neglect the effect of the phase relaxation of the $|1\rangle$-$|2\rangle$ transition. These

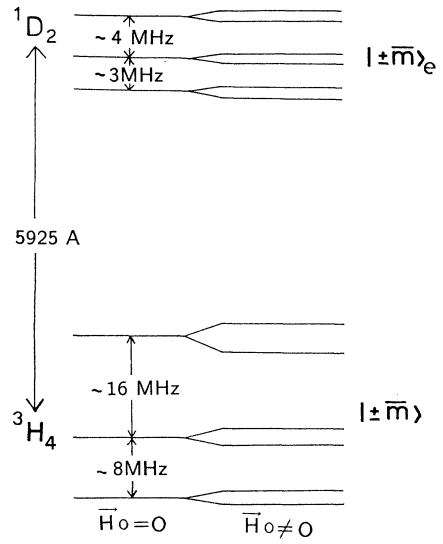

FIG. 3. Energy level diagram. $|+\overline{m}\rangle_{(e)}$ (or $|-\overline{m}\rangle_{(e)}$) represents the wave function of the state whose Zeeman shift is positive (or negative).

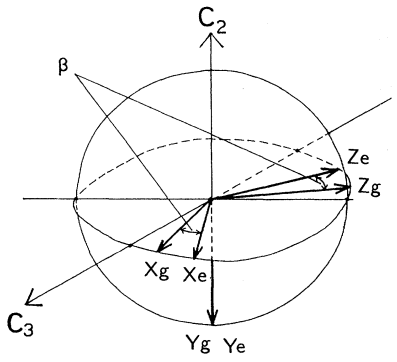

FIG. 4. Directions of the principal axes (X_g,Y_g,Z_g) and (X_e,Y_e,Z_e) of the ground- and excited-state quadrupole coupling tensors. $R(\alpha,\beta,\gamma)$ is the transformation operator from the system (X_e,Y_e,Z_e) to (X_g,Y_g,Z_g), where α, β, and γ are the Eulerian angles. The assignments of the principal axes are different from those in Ref. 2; ($\alpha=\gamma=0$).

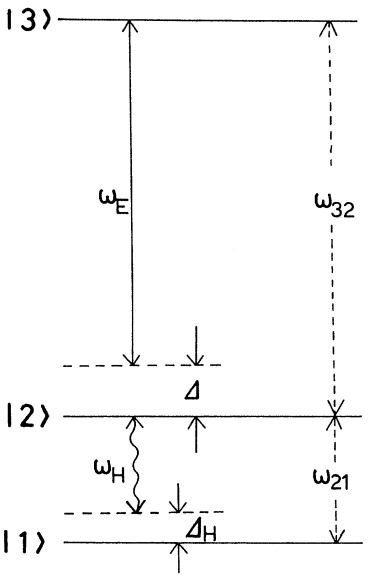

FIG. 5. Three-level system.

simplifications are not essential for the discussion of the symmetry properties of the RHS.

We derive the expression of the RHS induced by the application of the probe light to the system where the sublevel coherence (spin echoes generated by the application of two rf pulses) exists between levels $|1\rangle$ and $|2\rangle$, and there is no optical coherence and no population in the optically excited state. In our experiment the creation of sublevel population difference by optical pumping, the generation of sublevel coherence by rf pulses, and the detection of the coherence by a probe light are performed at different times. This makes the analysis simpler than that in the experiment[1,2] using cw irradiation and a rapid frequency sweeping of the laser light. The optical pumping process and the effect of level multiplicity will be discussed later.

By solving the density matrix equation for the three-level system we obtain Eq. (A15) for the Raman heterodyne beat signal as

$$I_s(t)=-2\pi k_E LN(b+b')|E_p|^2\mathrm{Re}[-i\sigma^{(3)}\exp(i\omega_H t)] . \tag{3.1}$$

The derivation is described in detail in the Appendix. The procedure to obtain this expression is a little more rigorous than that in Ref. 1. It is evident that the characteristics of the RHS after the phase-sensitive detection of $I_s(t)$ are represented by

$$S=a|E_p|^2\sigma^{(3)} , \tag{3.2}$$

where a is a real constant given by $-2\pi k_E LN(b+b')$. Hereafter we call S the RHS. Equation (3.2) shows that RHS is proportional to the probe light intensity and $\sigma^{(3)}$.[1,2] $\sigma^{(3)}$ is a product of the transition matrix elements relevant to the coherent Raman process; $\sigma^{(3)}=\mu_{12}\mu_{23}\mu_{31}$. It is in general a complex quantity involving the phase of the signal.

The laser frequency jitter ($\sim$3 MHz) is quite small compared to the rf transition frequencies ($\sim$8 MHz and $\sim$16 MHz). Therefore in our case the anti-Stokes process ($\Delta\sim 0$) and Stokes process ($\Delta\sim-\omega_{21}$) are treated separately. Constants b and b' correspond to these two processes. Equation (3.2) shows that RHS vanishes if $b+b'=0$. This occurs when the population differences $\rho_{22}-\rho_{11}$ for these two processes created by the pump pulse are just inverted with each other and therefore the sublevel coherences detected by these processes are of the same amplitude and 180° out of phase [see Eq. (A14)]. It is also worthwhile to note that these two processes give the same RHS ($b=b'$) when the relevant sublevel coherences are the same.

We have dealt with the RHS of spin echoes. In the case of the cw signals[1,2] the symmetry properties are also determined by $\sigma^{(3)}$ and the discussion of the symmetry properties should be the same.

In Pr^{3+}:LaF_3 the state $|i\rangle$ can be factored into the nuclear and electronic parts, $|i\rangle=|i_{\mathrm{nu}}\rangle|i_{\mathrm{el}}\rangle$, where $|1_{\mathrm{el}}\rangle$ and $|2_{\mathrm{el}}\rangle$ are equal to $|\phi_g\rangle$ and $|3_{\mathrm{el}}\rangle=|\phi_e\rangle$. Therefore $\sigma^{(3)}$ is also factored into nuclear and electronic parts. The electronic part of $\sigma^{(3)}$ equal to $|\langle\phi_g|\mathbf{e}_p\cdot\mathbf{d}_e|\phi_e\rangle|^2$ and is a real constant. It does not depend on the particular choice of the levels $|1\rangle$, $|2\rangle$, and $|3\rangle$. Therefore in later analysis we only consider the nuclear part of $\sigma^{(3)}$.

IV. INTERPRETATION BY GEOMETRICAL SYMMETRY

In some special situations, the observed symmetry properties can be explained only from the consideration of the geometrical symmetry of the system.

The first example is the symmetry property (4) in Table I. In Fig. 6(a) we show the geometrical situations. In the left figure the static magnetic field $\mathbf{H}_0(\perp\mathbf{C}_3)$ is applied making an angle $+\theta$ with respect to the C_2 axis. The rf field $\mathbf{H}_1(t)$ is along the C_3 axis ($+X$ direction). We denote the RHS in this situation $S(\theta)$. In the right figure a different situation is shown where the angle between $\mathbf{H}_0(\perp\mathbf{C}_3)$ and the C_2 axis is $-\theta$ [referring to the original coordinate (X,Y,Z)]. We denote the RHS in this situation $S(-\theta)$. The symmetry property (4) means that $S(\theta)=-S(-\theta)$.

To explain this relation we introduce, in the right figure, a new coordinate system (X',Y',Z') which is obtained by 180° rotation of the system (X,Y,Z) about the C_2 axis. The Pr^{3+} ions seen from these two coordinates are identical since the local symmetry at the Pr^{3+} site is C_2,[11] but the directions of the external fields seen from these coordinates are different. Referring to the coordinate (X',Y',Z'), $\mathbf{H}_0$ makes an angle $+\theta$ to the C_2 axis, and $\mathbf{H}_1$ is along the $-X'$ direction. Suppose that the phase of the rf field is shifted by 180° or the direction of $\mathbf{H}_1$ is inverted. In this "virtual" situation the physical condition of the system seen from the coordinate (X',Y',Z') is identical to that seen from the coordinate (X,Y,Z) in the left figure. Therefore this virtual situation should yield the RHS equal to that in the left figure, namely, $S(\theta)$. In the real situation in the right figure, the

phase of the rf field is different by 180° from that in the virtual situation, and therefore the RHS $S(-\theta)$ should be equal to $-S(\theta)$. This is the explanation of the symmetry properties (4).

When both $\mathbf{H}_0$ and $\mathbf{H}_1$ are parallel to the C_3 axis, the symmetry property (1) can be explained in a similar way. We denote the RHS in the left figure in Fig. 6(b) $S(\mathbf{H}_0)$. $\mathbf{H}_0$ is inverted in the right figure and we denote the RHS $S(-\mathbf{H}_0)$. If $\mathbf{H}_1$ is also inverted in the right figure, the physical situation seen from the (X',Y',Z') system becomes identical to that in the left figure, and the RHS equal to $S(\mathbf{H}_0)$ should be observed. Therefore the situation in the right figure should give the RHS $-S(\mathbf{H}_0)$, namely, $S(-\mathbf{H}_0)=-S(\mathbf{H}_0)$. This is the explanation.

The symmetry property (3) is the direct consequence of the symmetry property (1), and the symmetry property (2) when $\mathbf{H}_0\|\mathbf{C}_3$ is self-evident since A and B sites are equivalent in this case. Thus we have explained all of the symmetry properties in the first group.

V. GENERAL SYMMETRY LAW FOR RHS

In this section we theoretically derive a general symmetry law of RHS for magnetic field reversal using the expression of RHS and the property of the rotation matrix $D^{(5/2)}_{i,j}(\alpha,\beta,\gamma)$.[9,10] The law holds for arbitrary directions of the quadrupole axes of the ground and excited states and of the rf and static magnetic fields.

In order to derive the law, we first consider the wave functions of the ground- and excited-state sublevels. For the ground state these are expressed as

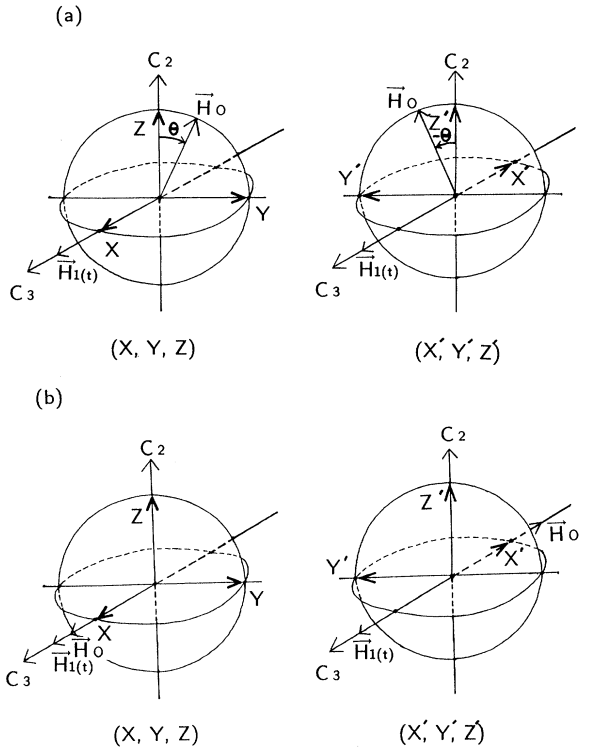

FIG. 6. Diagrams for the geometrical interpretation of the symmetry property. (X,Y,Z) and (X',Y',Z') are two principal coordinate systems which are interchanged by 180° rotation about the C_2 axis. (a) is to explain the symmetry property for $\theta\leftrightarrow-\theta$ where θ is the angle between the $\mathbf{C}_2$ axis and $\mathbf{H}_0(\perp\mathbf{C}_3)$, and (b) is for the magnetic field reversal when $\mathbf{H}_0\|\mathbf{C}_3$.

$$
\begin{aligned}
|+\bar{m}\rangle &= \exp(i\pi/4)[-\exp(-i\xi_m/2)\sin(\alpha_m)|+m\rangle+\exp(+i\xi_m/2)\cos(\alpha_m)|-m\rangle]\ ,\\
|-\bar{m}\rangle &= \exp(-i\pi/4)[(\exp(-i\xi_m/2)\cos(\alpha_m)|+m\rangle+\exp(+i\xi_m/2)\sin(\alpha_m)|-m\rangle]\ ,
\end{aligned}
\quad (m=\tfrac{5}{2},\ \tfrac{1}{2},\ -\tfrac{3}{2})\ . \tag{5.1}
$$

where the ground-state quadrupole axes are taken as the quantization axes. $|+\bar{m}\rangle$ (or $|-\bar{m}\rangle$) denotes the wave function of the level whose energy shift by the weak magnetic field is positive (or negative). Notations α_m, ξ_m, and $|\pm m\rangle$ corresponds to α_i, ξ_i, and $|\pm m_i\rangle$ in Ref. 2, respectively.[12] The polar coordinates (θ,ϕ) of a static magnetic field with respect to the quantization axes are involved in α_m and ξ_m.

The excited-state wave functions can be written in the same form as in Eq. (5.1) by using quantities $\alpha_{m'}$, $\xi_{m'}$, $|\pm m\rangle'$, and (θ',ϕ') for the excited state in which the excited-state quadrupole axes are taken as the quantization axes. The expressions when the ground-state quadrupole axes are taken as quantization axes can be obtained by using the rotation matrix $D^{(5/2)}_{i,j}(\alpha,\beta,\gamma)$ (Refs. 9 and 10) as

$$
\begin{aligned}
|+\bar{m}\rangle_e &= \exp(i\pi/4)[-\exp(-i\xi_{m'}/2)\sin(\alpha_{m'})|+m\rangle_e+\exp(+i\xi_{m'}/2)\cos(\alpha_{m'})|-m\rangle_e]\ ,\\
|-\bar{m}\rangle_e &= \exp(-i\pi/4)[\exp(-i\xi_{m'}/2)\cos(\alpha_{m'})|+m\rangle_e+\exp(+i\xi_{m'}/2)\sin(\alpha_{m'})|-m\rangle_e]\ ,
\end{aligned}
\quad (m=\tfrac{5}{2},\ \tfrac{1}{2},\ -\tfrac{3}{2}) \tag{5.2}
$$

with

$$
|\pm m\rangle_e=\sum_{n,n'=\pm5/2,\pm3/2,\pm1/2}|\tfrac{5}{2},n\rangle D^{(5/2)}_{n,n'}(\alpha,\beta,\gamma)\langle\tfrac{5}{2},n'|\pm m\rangle'\ , \tag{5.3}
$$

where α, β, and γ are Eulerian angles for the transformation from the excited-state quadrupole axes to the ground-state ones. $|\frac{5}{2},n\rangle$ is the eigenstate of I_z with eigenvalue n and is equal to ψ_n in Ref. 2.

Using the relation[9]

$$
[D^{(5/2)}_{i,j}(\alpha,\beta,\gamma)]^*=(-1)^{i-j}D^{(5/2)}_{-i,-j}(\alpha,\beta,\gamma)\ , \tag{5.4}
$$

we can obtain simple relations between the transition matrix elements. For the optical transition we obtain

$$\langle +\bar{m}|\pm\bar{n}\rangle_e=\pm(\langle -\bar{m}|\mp\bar{n}\rangle_e)^* \quad (m,n=\tfrac{5}{2},\ \tfrac{1}{2},\ -\tfrac{3}{2}) . \tag{5.5}$$

These relations indicate that the optical transition probability between the levels $|+\bar{m}\rangle$ and $|\pm\bar{n}\rangle_e$ is equal to that between the levels $|-\bar{m}\rangle$ and $|\mp\bar{n}\rangle_e$. In a similar way we obtain

$$\langle +\bar{m}|\mathbf{A}\cdot\mathbf{I}|\pm\bar{m}'\rangle=\mp(\langle -\bar{m}|\mathbf{A}\cdot\mathbf{I}|\mp\bar{m}'\rangle)^* , \tag{5.6}$$

for the rf transition, where $\mathbf{A}=\hbar\mathbf{e}_{\mathbf{H}_1}\cdot\gamma_N$ and γ_N is the nuclear gyromagnetic ratio tensor.

Now we consider the inversion of the direction of the static magnetic field. It is represented by the transformation

$$(\theta^{(,)},\phi^{(,)})\rightarrow(\pi-\theta^{(,)},\phi^{(,)}+\pi) \tag{5.7}$$

As for ${\alpha_m}^{(,)}$ and ${\xi_m}^{(,)}$ the transformations are

$${\alpha_m}^{(,)}(-\mathbf{H}_0)=\pi/2-{\alpha_m}^{(,)}(\mathbf{H}_0) , \tag{5.8}$$

$${\xi_m}^{(,)}(-\mathbf{H}_0)=\pi+{\xi_m}^{(,)}(\mathbf{H}_0) . \tag{5.9}$$

Therefore we obtain from (5.1) and (5.2)

$$\langle\pm\bar{m}|\pm\bar{n}\rangle_e(-\mathbf{H}_0)=[\langle\pm\bar{m}|\pm\bar{n}\rangle_e(\mathbf{H}_0)]^* , \tag{5.10}$$

for the optical transition, and

$$\langle\pm\bar{m}|\mathbf{A}\cdot\mathbf{I}|\pm\bar{m}'\rangle(-\mathbf{H}_0)=-[\langle\pm\bar{m}|\mathbf{A}\cdot\mathbf{I}|\pm\bar{m}'\rangle(\mathbf{H}_0)]^* \tag{5.11}$$

for the rf transition, where $\langle +\bar{m}|+\bar{n}\rangle(\pm\mathbf{H}_0)$, etc., denote the values of the matrix elements at $\pm\mathbf{H}_0$.

It might be considered that the different relations would be obtained if different phase factors are adopted in the expressions for the wave functions Eqs. (5.1) and (5.2). But the product of the three-matrix elements $(\mu_{12}\mu_{23}\mu_{31})$ is independent of the phase factors.

In Sec. III we have shown that the RHS is proportional to the product of the three-matrix elements $\mu_{12}\mu_{23}\mu_{31}$ and it determines the phase of the signal. Now we derive the general symmetry law using the relations obtained in the above. The product $\sigma^{(3)}$ can be written explicitly as

$$\sigma^{(3)}(\mathbf{H}_0;\pm\bar{m},\pm\bar{m}',\pm\bar{n}) \equiv\langle\pm\bar{m}|\mathbf{A}\cdot\mathbf{I}|\pm\bar{m}'\rangle(\mathbf{H}_0) \times\langle\pm\bar{m}'|\pm\bar{n}\rangle_e(\mathbf{H}_0)_e\langle\pm\bar{n}|\pm\bar{m}\rangle(\mathbf{H}_0) . \tag{5.12}$$

Thus we obtain from Eqs. (5.10), (5.11), and (5.12)

$$\sigma^{(3)}(-\mathbf{H}_0;\pm\bar{m},\pm\bar{m}',\pm\bar{n}) =-[\sigma^{(3)}(\mathbf{H}_0;\pm\bar{m},\pm\bar{m}',\pm\bar{n})]^* . \tag{5.13}$$

This is the general symmetry law, and is a kind of reciprocal relation connecting the signals before and after the magnetic field reversal. It governs the phase change of the signal for the magnetic field reversal. Namely, if $\sigma^{(3)}$ is real the signal changes its sign for the magnetic field reversal, and if $\sigma^{(3)}$ is pure imaginary the signal is unchanged. The observed symmetry property for the magnetic field reversal can be explained if we are able to know the nature of $\sigma^{(3)}$. In Sec. VI we examine the nature of $\sigma^{(3)}$ by using a simple transition diagram and in Sec. VII by numerical calculations.

The general symmetry law can be derived from more general viewpoints, the time-reversal symmetry, especially the antilinearity of the time-reversal operation and the sign reversal of spins by the time-reversal transformation. The law is generally applicable to the signals in any phase-sensitive magnetic sublevel spectroscopies. The derivation of the law and its applications will be described elsewhere.

Using Eqs. (5.5), (5.6), and (5.13) we can obtain the relation

$$\sigma^{(3)}(-\mathbf{H}_0;\pm\bar{m},\pm\bar{m}',\pm\bar{n}) =\sigma^{(3)}(\mathbf{H}_0;\mp\bar{m},\mp\bar{m}',\mp\bar{n}) . \tag{5.14}$$

This relation indicates that the symmetry property (3) for the Zeeman spectra ξ and η can be explained on the same basis as that for the magnetic field reversal.

VI. EXPLANATION USING SIMPLE TRANSITION DIAGRAMS

In this section we explain the symmetry property for magnetic field reversal when $\mathbf{H}_0\perp\mathbf{C}_3$, using the general symmetry law and simplified transition diagrams. As is shown in Table I, 16-MHz signals change their signs whereas 8-MHz ones do not, when the direction of the magnetic field is reversed.[2,5] This fact can be explained if we are able to show that $\sigma^{(3)}$ is real for 16-MHz signals and pure imaginary for 8-MHz ones. To show this we consider the transition diagrams as shown in Figs. 7(a) and 7(b).

Both the ground and excited states are subjected to the nonaxial quadrupole interactions (see Fig. 4). The ground-state quadrupole interaction is less asymmetrical than that of the excited state. Therefore we take quanti-

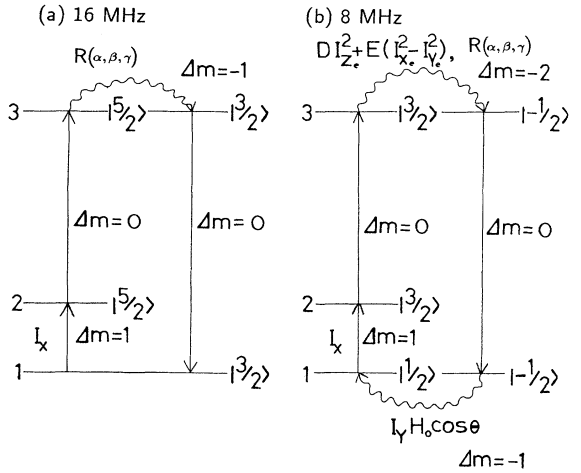

FIG. 7. Simplified transition diagrams. (a) and (b) are for the 16- and 8-MHz transitions, respectively.

zation axes along the ground-state quadrupole axes so that the ground-state sublevels can be well specified by the nuclear magnetic quantum number m (I_z can be considered to be a good quantum number) in the absence of the static magnetic field. For simplicity, we use the approximation that the ground-state quadrupole X axis is parallel to the C_3 axis. Therefore I_x is responsible for the rf transition (see Fig. 4).

The Zeeman splittings of the excited state sublevels for $\mathbf{H}_0$ (<100 Oe) are small (less than about 2 MHz) compared to the spectral width of our laser (~ 3 MHz). Therefore we treat the excited-state Zeeman sublevels as degenerate ones.

Figure 7(a) shows the transition diagram for the 16-MHz signals. The arrows indicate optical and rf transitions involved in the Raman heterodyne process and the wavy arrow the existence of the state mixing. The selection rule for the nuclear magnetic quantum number for the optical transition is $\Delta m=0$ and that for the rf transition is $\Delta m=1$. Matrix elements for these transitions are real (we can take $\langle m|I_x|m'\rangle$ as real without loss of generality[9]). Because the selection rule for the total process should be $\Delta m=0$, the mixing $\Delta m=-1$ in level 3 must be incorporated to close the loop. The state mixing $\Delta m=-1$ is caused by the incongruence between the ground- and excited-state quadrupole axes, and the mixing coefficient is real because α and γ is zero[9] (see Fig. 4). Thus the product of the matrix elements involved in this closed path is real. Because this is considered to be the dominant process involved in the 16-MHz signals, $\sigma^{(3)}$ is almost real for the 16-MHz signals.

Figure 7(b) is the transition diagram for the 8-MHz signals. The main difference from the 16-MHz case is that the ground-state 1 is not a nearly pure state, but a mixture of $|\frac{1}{2}\rangle$ and $|-\frac{1}{2}\rangle$ due to the Zeeman interaction with a static magnetic field. The state 2 is nearly pure $|\frac{3}{2}\rangle$. Considering the selection rule $\Delta m=0$ for the total process the mixing $\Delta m=-2$ in level 3 is necessary in this case. The mixing can be provided by the nonaxial quadrupole interaction of the form $DI_{Ze}^2+E(I_{Xe}^2-I_{Ye}^2)$ and also by the incongruence between the ground- and excited-state quadrupole axes. The relevant matrix elements are also real. But in the state mixing $\Delta m=1$ in the ground-state 1 the factor "$i\cos(\theta)$" is introduced where θ is an angle between the static magnetic field and the C_2 axis ($\langle m|I_Y|m'\rangle$ is pure imaginary[9]). Because this process is considered to be dominant, $\sigma^{(3)}$ is almost pure imaginary in the 8-MHz case.

Thus we have explained the difference between the symmetry properties for 16- and 8-MHz transitions for the magnetic field reversal when $\mathbf{H}_0\perp\mathbf{C}_3$.

VII. INTERPRETATION BY NUMERICAL CALCULATIONS

We have discussed symmetry properties considering a simple three-level system. However, the observed signals are the sum of the contributions from many three-level systems. Population differences in the ground-state sublevels created by optical pumping and the nature of $\sigma^{(3)}$ are generally different for these three-level systems. The symmetry properties belonging to the first group in Table I are determined regardless of these effects as shown in Sec. IV. The symmetry properties belonging to the second group may depend on these effects. In Sec. VI we have given a qualitative explanation using simple transition diagrams. In this section we give the more quantitative explanation for the symmetry properties in the second group by performing numerical calculations considering the existence of many three-level systems. The validity of the general symmetry law derived in Sec. V is also confirmed by this calculation.

In order to explain the observed symmetry properties by using numerical calculations, we first consider the optical pumping in the multilevel system.

A. Creation of sublevel population difference

Population differences between the ground-state sublevels are created by the optical pumping pulse. The optical pumping effect in Pr^{3+}:LaF_3 is very complicated and may sensitively depend on the pumping conditions such as the pumping power and the spectral width of the pumping light. The details of the pumping process are not known. Here we make plausible assumptions that (1) the depopulation from the magnetic sublevels of $^3H_4$ to those of $^1D_2$ occurs proportional to the optical transition probabilities between these sublevels and (2) there is no nuclear spin memory, that is, the repopulation from $^1D_2$ to $^3H_4$ does not depend on the magnetic sublevels.

The frequency jitter of the laser we used is about 3 MHz, and the frequency splittings of magnetic sublevels by $\mathbf{H}_0$ (≤ 100 Oe) are at most 2 MHz in $^1D_2$ state. Therefore we assume that the excited-state magnetic sublevels can be treated as degenerated ones during the optical pumping process.

B. Incorporation of multilevel effect

There are six sublevels in each of $^1D_2$ and $^3H_4$ states. Therefore 12 ($=2\times 6$) independent transitions (6 anti-Stokes and 6 Stokes processes) take part in the signal because of the large inhomogeneous broadening of $^1D_2$-$^3H_4$ transition (~ 5 GHz). Therefore we obtain the expression S_t for the total RHS as

$$S_t=a'|E_p|^2\sum_{m=5/2,1/2,-3/2}\{[b(+\bar{m})+b'(+\bar{m})]\sigma^{(3)}(+\bar{m})+[b(-\bar{m})+b'(-\bar{m})]\sigma^{(3)}(-\bar{m})\}\ , \tag{7.1}$$

where $a'=-2\pi k_E LN$, and $\sigma^{(3)}(\pm\bar{m})$ and $b^{(\prime)}(\pm\bar{m})$ represent the values of $\mu_{12}\mu_{23}\mu_{31}$ and $b^{(\prime)}$, respectively, when level 3 is $|\pm\bar{m}\rangle_e$. We have assumed that the excited-state magnetic sublevels can be regarded as degenerate ones during the optical pumping process and that the sublevel population differences are created by the pumping pulse in proportion to the transition probability of the transition resonant to the pumping pulse. Therefore the values of $b(\pm\bar{m})$ and $b'(\pm\bar{m})$ can be obtained by using Eq. (A14):

$$b(+\overline{m})=b(-\overline{m})=(|\langle 2|+\overline{m}\rangle_e|^2+|\langle 2|-\overline{m}\rangle_e|^2)b_0\ , \tag{7.2}$$

$$b'(+\overline{m})=b'(-\overline{m})=(|\langle 1|+\overline{m}\rangle_e|^2+|\langle 1|-\overline{m}\rangle_e|^2)b'_0\ , \tag{7.3}$$

where b_0 and b'_0 are constants independent of the transition matrix elements. Inserting Eqs. (7.2) and (7.3) into Eq. (7.1) we obtain,

$$S_t=a'|E_p|^2 \sum_{m=5/2,1/2,-3/2} [\sigma^{(3)}(+\overline{m})+\sigma^{(3)}(-\overline{m})] \times[b_0(|\langle 2|+\overline{m}\rangle_e|^2+|\langle 2|-\overline{m}\rangle_e|^2)+b'_0(|\langle 1|+\overline{m}\rangle_e|^2+|\langle 1|-\overline{m}\rangle_e|^2)]\ . \tag{7.4}$$

In the expression of $\sigma^{(3)}(+\overline{m})+\sigma^{(3)}(-\overline{m})$ the projection operator $|+\overline{m}\rangle_{ee}\langle+\overline{m}|+|-\overline{m}\rangle_{ee}\langle-\overline{m}|$ appears. It can be calculated from Eq. (5.2) and is equal to $|+m\rangle_{ee}\langle+m|+|-m\rangle_{ee}\langle-m|$ which is independent of the static magnetic field.

Equation (7.4) is the final expression of RHS used for the numerical calculations.

C. Results of numerical calculations

The results of the numerical calculation of the real and imaginary parts of expression (7.4) are shown in Fig. 8 where the parameters in Ref. 2 are used[12] and we assumed that $b'_0=-b_0$ for simplicity. θ is an angle between the C_2 axis and the applied static magnetic field which is perpendicular to the C_3 axis. The rf magnetic field is parallel to the C_3 axis. The numerical calculations give nearly real and pure imaginary values of S_t for the 16- and 8-MHz signals, respectively. This is just expected from the discussion in Sec. VI. The angular dependence of $\sigma^{(3)}$ for 8-MHz signals is roughly represented as $\cos(\theta)$ given in the discussion in Sec. VI. When $\theta=0°$ or 180° ($\mathbf{H}_0\|\mathbf{C}_2$), the signal vanishes both for 16- and 8-MHz transitions. This can be explained by the geometrical consideration similar to that in Sec. IV. When θ is 90° ($\mathbf{H}_0\perp\mathbf{C}_2$), the imaginary part vanishes, which is also explained geometrically. The results of numerical calculation also show that S_t actually obeys the general symmetry law [Eq. (5.13)].

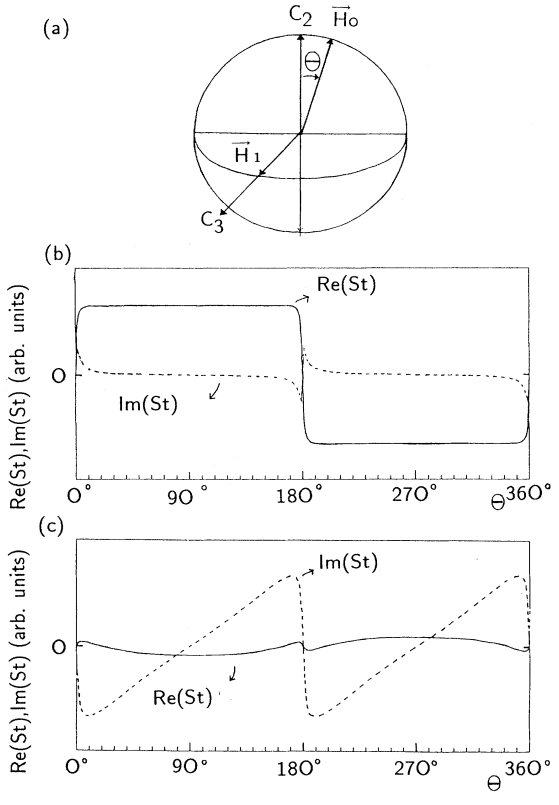

FIG. 8. Results of numerical calculations. The angle θ is between the $\mathbf{C}_2$ axis and $\mathbf{H}_0(\perp\mathbf{C}_3)$. The rf magnetic field is parallel to the $\mathbf{C}_3$ axis.

VIII. PREDICTION FOR OTHER CONDITIONS

We have dealt with the cases where $\mathbf{H}_1\|\mathbf{C}_3$ in Pr^{3+}:LaF_3. It is possible to predict the symmetry properties when $\mathbf{H}_1\perp\mathbf{C}_3$ from similar arguments. The predictions are shown in Table II. As is expected from the geometrical symmetry, the relative direction of $\mathbf{H}_1$ with respect to the C_2 axis is important. We consider two cases where $\mathbf{H}_1\|\mathbf{C}_2$ [Table II(a)] and $\mathbf{H}_1\perp\mathbf{C}_2$ [Table II(b)].

Some of the symmetry properties (indicated by an asterisk) are derived only from the geometrical consideration as in the case of $\mathbf{H}_1\|\mathbf{C}_3$. The other symmetry properties are expected from the observed symmetry properties in the case of $\mathbf{H}_1\|\mathbf{C}_3$. Optical pumping processes are independent of $\mathbf{H}_1$. The rf transition matrix elements in the case of $\mathbf{H}_1\|\mathbf{C}_2$ are proportional to $\langle m|I_Y|m'\rangle$ whereas those in the case of $\mathbf{H}_1\perp\mathbf{C}_3$ to $\langle m|I_X|m'\rangle$. Since $\langle m|I_Y|m'\rangle$ is pure imaginary and $\langle m|I_X|m'\rangle$ is real, the phase of $\sigma^{(3)}$ for $\mathbf{H}_1\|\mathbf{C}_2$ differs by $\pi/2$ from that for $\mathbf{H}_1\perp\mathbf{C}_3$. Therefore we can expect by using the general symmetry law that the symmetry property (odd or even) for the magnetic field reversal when $\mathbf{H}_1\|\mathbf{C}_2$ is opposite to that when $\mathbf{H}_1\perp\mathbf{C}_3$. The other symmetry properties can be expected in the similar way.

Symmetry properties of Pr^{3+}:$YAlO_3$ observed by Mitsunaga *et al.*[2] and of Eu^{3+}:$YAlO_3$ observed by Erickson[6] will also be able to be explained in the similar way.

TABLE II. Expected symmetry properties in the case of $\mathbf{H}_1 \perp \mathbf{C}_3$, and $\mathbf{H}_1 \| \mathbf{C}_2$ in (a) and $\mathbf{H}_1 \perp \mathbf{C}_2$ in (b). The notation is the same as that in Table I.

(a) $\vec{H}_1 \| \vec{C}_2$

rf transition	(1) field reversal $\vec{H}_o \longleftrightarrow -\vec{H}_o$		(2) site interchange *Asite* $\longleftrightarrow$ *Bsite*		(3) Zeeman spectra $\xi \longleftrightarrow \eta$		(4) $\theta \equiv \angle(\vec{H}_o, \vec{C}_2)$ $\theta \longleftrightarrow -\theta$
	$\vec{H}_o \perp \vec{C}_3$	$\vec{H}_o \| \vec{C}_3^*$	$\vec{H}_o \perp \vec{C}_3$	$\vec{H}_o \| \vec{C}_3^*$	$\vec{H}_o \perp \vec{C}_3$	$\vec{H}_o \| \vec{C}_3^*$	$\vec{H}_o \perp \vec{C}_3^*$
$\pm\frac{3}{2} \leftrightarrow \pm\frac{5}{2}$ ($\sim 16MHz$)	even	even	odd	odd	even	even	even
$\pm\frac{1}{2} \leftrightarrow \pm\frac{3}{2}$ ($\sim 8MHz$)	odd	even	even	odd	odd	even	even

(b) $\vec{H}_1 \perp \vec{C}_2$

rf transition	(1) field reversal $\vec{H}_o \longleftrightarrow -\vec{H}_o$		(2) site interchange *Asite* $\longleftrightarrow$ *Bsite*		(3) Zeeman spectra $\xi \longleftrightarrow \eta$		(4) $\theta \equiv \angle(\vec{H}_o, \vec{C}_2)$ $\theta \longleftrightarrow -\theta$
	$\vec{H}_o \perp \vec{C}_3$	$\vec{H}_o \| \vec{C}_3^*$	$\vec{H}_o \perp \vec{C}_3$	$\vec{H}_o \| \vec{C}_3^*$	$\vec{H}_o \perp \vec{C}_3$	$\vec{H}_o \| \vec{C}_3^*$	$\vec{H}_o \perp \vec{C}_3^*$
$\pm\frac{3}{2} \leftrightarrow \pm\frac{5}{2}$ ($\sim 16MHz$)	odd	odd	even	odd	odd	odd	odd
$\pm\frac{1}{2} \leftrightarrow \pm\frac{3}{2}$ ($\sim 8MHz$)	even	odd	odd	odd	even	odd	odd

IX. SUMMARY

In summary we observed various symmetry properties of the RHS in Pr^{3+}:LaF_3 and explained all of them using the general symmetry law which we have theoretically derived and geometrical symmetries. The numerical calculation gives quantitative explanation of the observed symmetry properties.

APPENDIX: DERIVATION OF Eq. (3.1)

RHD is a technique to optically detect sublevel coherence through coherent resonant Raman scattering. We derive the expression of RHS induced by the probe light. For that purpose we solve the density matrix equation of motion under the initial condition that the sublevel coherence is already generated by the rf pulses and there is no optical coherence and no population in the optically excited state.

1. Density-matrix formula

The interaction between a three-level system and the probe field

$$\mathbf{E}_p(t,z)=\mathbf{e}_p E_p \exp(+i\omega_E t - ik_E z)/2 + \text{c.c.}$$

can be expressed by the density matrix formula. The direction of the probe beam is taken along the z axis, $\mathbf{e}_p$ is the unit vector which expresses the direction of the polarization, and $\mathbf{E}_p$ is taken to be real. The density matrix equations for the three-level system in Fig. 5 are as follows:

$$\dot{\tilde{\rho}}_{12}(t,\Delta)=(i/2)[\chi_{13}\tilde{\rho}_{32}(t,\Delta)-\chi_{32}\tilde{\rho}_{13}(t,\Delta)]\exp(-i\omega_H t)\ , \tag{A1a}$$

$$\dot{\tilde{\rho}}_{13}(t,\Delta)=[i(\Delta+\omega_N)-\gamma_t]\tilde{\rho}_{13}(t,\Delta)+i(\chi_{13}/2)[\rho_{33}(t,\Delta)-\rho_{11}(t,\Delta)]-i(\chi_{23}/2)\tilde{\rho}_{12}(t,\Delta)\exp(+i\omega_H t)\ , \tag{A1b}$$

$$\dot{\tilde{\rho}}_{23}(t,\Delta)=(i\Delta-\gamma_t)\tilde{\rho}_{23}(t,\Delta)+i(\chi_{23}/2)[\rho_{33}(t,\Delta)-\rho_{22}(t,\Delta)]-i(\chi_{13}/2)\tilde{\rho}_{21}(t,\Delta)\exp(-i\omega_H t) \tag{A1c}$$

where γ_t is the optical dephasing rate, χ_{i3} is the Rabi frequency for the $i-3$ transition ($i=1,2$), and the tilde denotes the slowly varying part as

$$\rho_{12}(t,\Delta)=\tilde{\rho}_{12}(t,\Delta)\exp(+i\omega_H t)\ , \tag{A2a}$$

$$\rho_{13}(t,z,\Delta)=\tilde{\rho}_{13}(t,\Delta)\exp[+i(\omega_E t-k_E z)]\ , \tag{A2b}$$

$$\rho_{23}(t,z,\Delta)=\tilde{\rho}_{23}(t,\Delta)\exp[+i(\omega_E t-k_E z)]\ . \tag{A2c}$$

2. Detection of sublevel coherence

The initial conditions are

$$\tilde{\rho}_{13}(0,\Delta)=\tilde{\rho}_{23}(0,\Delta)=\rho_{33}(0,\Delta)=0\ , \tag{A3a}$$

$$\tilde{\rho}_{12}(0,\Delta)\neq 0\ , \tag{A3b}$$

namely, at $t=0$ (at the beginning of the probe pulse)

there is no optical coherence and no population in the optically excited state but sublevel coherence exists. The sample with sublevel coherence $\tilde{\rho}_{12}(0,\Delta)$ causes a coherent Raman scattering of the probe light.

a. Anti-Stokes process ($\Delta\sim 0$). When the probe light E_p is nearly tuned to the 2-3 transition, $\tilde{\rho}_{13}(t,\Delta)$ is oscillating at the frequency nearly equal to ω_H whereas $\tilde{\rho}_{23}(t,\Delta)$ is not. From Eqs. (A1a) and (A1b) we obtain

$$\dot{\tilde{\rho}}_{12}(t,\Delta)=-i(\chi_{32}/2)\bar{\rho}_{13}(t,\Delta)\ , \tag{A4a}$$

$$\dot{\bar{\rho}}_{13}(t,\Delta)=(i\Delta-\gamma_t)\bar{\rho}_{13}(t,\Delta) -i(\chi_{23}/2)\tilde{\rho}_{12}(t,\Delta)\ , \tag{A4b}$$

where $\bar{\rho}_{13}(t,\Delta)=\tilde{\rho}_{13}(t,\Delta)\exp(-i\omega_H t)$ and rapidly oscillating terms are neglected.

Considering the initial conditions we obtain $\bar{\rho}_{13}(t,\Delta)$ from Eqs. (A4a) and (A4b) as

$$\bar{\rho}_{13}(t,\Delta)=\frac{-i\chi_{23}\tilde{\rho}_{12}(0,\Delta)}{\sqrt{|\chi_{23}|^2+\Delta^2-\gamma_t^2+2i\gamma_t\Delta}}\exp[(-\gamma_t+i\Delta)t/2]\sin(\sqrt{|\chi_{23}|^2+\Delta^2-\gamma_t^2+2i\gamma_t\Delta}\,t/2)\ . \tag{A5}$$

The macroscopic coherence $\bar{\rho}_{13}(t)$ can be obtained by summing $\bar{\rho}_{13}(t,\Delta)$ over the optical inhomogeneous broadening $G(\Delta)$, namely,

$$\bar{\rho}_{13}(t)=\int_{-\infty}^{+\infty}d\Delta\,\bar{\rho}_{13}(t,\Delta)G(\Delta)\ . \tag{A6}$$

b. Stokes process ($\Delta\sim-\omega_{21}$). Using similar procedures as in the anti-Stokes process we can obtain

$$\bar{\rho}_{32}(t,\Delta')=\frac{+i\chi_{31}\tilde{\rho}_{12}(0,\Delta')}{\sqrt{|\chi_{31}|^2+\Delta'^2-\gamma_t^2-2i\gamma_t\Delta'}}\exp[(-\gamma_t-i\Delta')t/2]\sin(\sqrt{|\chi_{31}|^2+\Delta'^2-\gamma_t^2-2i\gamma_t\Delta'}\,t/2\ , \tag{A7}$$

where $\Delta'=\Delta+\omega_H$ and $\bar{\rho}_{32}(t,\Delta')=\tilde{\rho}_{32}(t,\Delta')\exp(-i\omega_H t)$.

Similarly to Eq. (A6) we obtain

$$\bar{\rho}_{32}(t)=\int_{-\infty}^{+\infty}d\Delta'\bar{\rho}_{32}(t,\Delta')G(\Delta')\ . \tag{A8}$$

3. Sublevel coherence associated with spin echoes

We treat the RHS of spin echoes produced by the application of $\pi/2$ and π rf pulses after the population difference $\rho_{22}(\Delta)-\rho_{11}(\Delta)$ is created by optical pumping. The rf field is expressed as

$$\mathbf{H}_1(t)=\mathbf{e}_{\mathbf{H}_1}H_1\exp(+i\omega_H t)/2+\text{c.c.}\ ,$$

where $\mathbf{e}_{\mathbf{H}_1}$ is the unit vector representing the direction of $\mathbf{H}_1$. The rf Rabi frequency χ_{12} is defined as $\chi_{12}=\mu_{12}H_1/\hbar$ where

$$\mu_{12}=\langle 1|\mathbf{e}_{\mathbf{H}_1}\cdot\mathbf{d}_m|2\rangle \tag{A9}$$

and $\mathbf{d}_m$ is the magnetic dipole operator. The sublevel coherence $\tilde{\rho}_{12}(0,\Delta)$ associated with spin echoes can be obtained by the standard procedure[13] as

$$\tilde{\rho}_{12}(0,\Delta)=-i[\rho_{22}(\Delta)-\rho_{11}(\Delta)]\mu_{12}/(2|\mu_{12}|)\ , \tag{A10}$$

where the decay of the sublevel coherence is neglected.

The sublevel coherence $\tilde{\rho}_{12}(0,\Delta)$ has nonzero-value for Δ within the spectral width ($\sim$3 MHz) of the pump pulse.

4. Raman heterodyne signal

The Raman light $E_s(t,z)$ is connected with density matrix elements $\tilde{\rho}_{13}(t)=\bar{\rho}_{13}(t)\exp(i\omega_H t)$ and $\tilde{\rho}_{23}(t)=\bar{\rho}_{23}(t)\exp(i\omega_H t)$ by Maxwell equations as follows:

$$\begin{aligned}\mathbf{E}_s(t,z)&=\mathbf{e}_p E_s(t)\exp[i(\omega_E t-k_E z)]+\text{c.c.}\\&=\mathbf{e}_p\{-2\pi i k_E LN[\mu_{31}\tilde{\rho}_{13}(t)+\mu_{32}\tilde{\rho}_{23}(t)]\}\exp[i(\omega_E t-k_E z)]+\text{c.c.}\ ,\end{aligned} \tag{A11}$$

where L is the sample length, N is the impurity-ion number density; an optically thin sample is assumed. μ_{i3} is the optical transition matrix element defined as

$$\mu_{i3}=\langle i|\mathbf{e}_p\cdot\mathbf{d}_e|3\rangle$$

where $\mathbf{d}_e$ is the electric dipole operator ($i=1,2$).

The signal field $\mathbf{E}_s(t,z)$ and the probe field $\mathbf{E}_p(t,z)$ give rise to the total field

$$\mathbf{E}_t(t,z)=\mathbf{E}_p(t,z)+\mathbf{E}_s(t,z)\ .$$

From the total intensity $|\mathbf{E}_t|^2$, one obtains the observed heterodyne beat signal

$$I_s(t)=2\,\mathrm{Re}[E_s(t)E_p^*]=-2\pi k_E LE_p N\,\mathrm{Re}[i\mu_{31}\tilde{\rho}_{13}(t)+i\mu_{32}\tilde{\rho}_{23}(t)]\ . \tag{A12}$$

The first term expresses the anti-Stokes process and the second term the Stokes process.

From Eqs. (A5)–(A8) and (A10) we obtain

$$i\mu_{31}\tilde{\rho}_{13}(t)=-ib\mu_{12}\mu_{23}\mu_{31}E_p\exp(+i\omega_H t)\ , \tag{A13a}$$

$$i\mu_{32}\tilde{\rho}_{23}(t)=ib'^{*}\mu_{21}\mu_{13}\mu_{32}E_p\exp(-i\omega_H t)\ , \tag{A13b}$$

where

$$b=\frac{-1}{2|\mu_{12}|}\int_{-\infty}^{+\infty}d\Delta\exp\{(-\gamma_t+i\Delta)t/2\}G(\Delta)\frac{[\rho_{22}(\Delta)-\rho_{11}(\Delta)]\sin(\sqrt{|\chi_{23}|^2+\Delta^2-\gamma_t^2+2i\gamma_t\Delta}\,t/2)}{\sqrt{|\chi_{23}|^2+\Delta^2-\gamma_t^2+2i\gamma_t\Delta}} \tag{A14a}$$

and

$$b'=\frac{-1}{2|\mu_{12}|}\int_{-\infty}^{+\infty}d\Delta'\exp[(-\gamma_t-i\Delta')t/2]G(\Delta')\frac{[\rho_{22}(\Delta')-\rho_{11}(\Delta')]\sin(\sqrt{|\chi_{23}|^2+\Delta'^2-\gamma_t^2-2i\gamma_t\Delta'}\,t/2)}{\sqrt{|\chi_{23}|^2+\Delta'^2-\gamma_t^2-2i\gamma_t\Delta'}}\ . \tag{A14b}$$

It is reasonable to assume that the population differences $\rho_{22}(\Delta)-\rho_{11}(\Delta)$ and $\rho_{22}(\Delta')-\rho_{11}(\Delta')$ are even functions of Δ and Δ'. In this case one can easily show that b and b' are real [$G(\Delta)$ and $G(\Delta')$ are also assumed to be even functions of Δ and Δ'].

We obtain the expression for $I_s(t)$ from Eqs. (A12), (A13a), and (A13b) as

$$I_s(t)=-2\pi k_E LN(b+b')|E_p|^2\mathrm{Re}[-i\sigma^{(3)}\exp(+i\omega_H t)]\ , \tag{A15}$$

where $\sigma^{(3)}$ is a product of the transition matrix elements relevant to the coherent Raman processes; $\sigma^{(3)}=\mu_{12}\mu_{23}\mu_{31}$.

It might be considered that b and b' depend on time t and is modulated. However it is shown in Ref. 14, in the case of $\gamma_t=0$, that b and b' are essentially time independent when the condition $\Gamma\gg|\chi_{23}|,|\chi_{13}|$ is satisfied [Γ is the width of Δ where $\tilde{\rho}_{12}(0,\Delta)\neq 0$, in other words, the width of the hole burned by the pump pulse]. In our experiment the condition is satisfied and therefore b and b' are time independent.

[1] J. Mlynek, N. C. Wong, R. G. DeVoe, E. S. Kintzer, and R. G. Brewer, Phys. Rev. Lett. **50**, 993 (1983); N. C. Wong, E. S. Kintzer, J. Mlynek, R. G. DeVoe, and R. G. Brewer, Phys. Rev. B **28**, 4993 (1983).

[2] M. Mitsunaga, E. S. Kintzer, and R. G. Brewer, Phys. Rev. Lett. **52**, 1484 (1984); M. Mitsunaga, E. S. Kintzer, and R. G. Brewer, Phys. Rev. B **31**, 6947 (1985); E. S. Kintzer, M. Mitsunaga, and R. G. Brewer, *ibid.* **31**, 6958 (1985).

[3] D. R. Taylor, Opt. Commun. **52**, 204 (1984); P. D. Bloch, W. S. Brocklesby, R. T. Harley, and D. R. Taylor, J. Phys. C **7**, 523 (1985).

[4] Y. Takahashi, T. Tanaka, H. Hatanaka, Y. Fukuda, and T. Hashi, J. Lumin. **38**, 261 (1987).

[5] Y. Takahashi, K. Ishikawa, T. Tanaka, Y. Fukuda, H. Hatanaka, and T. Hashi, Phys. Rev. B **38**, 7121 (1988).

[6] L. E. Erickson, J. Phys. C **20**, 291 (1987).

[7] A. Szabo, T. Muramoto, and R. Kaarli, Opt. Lett. **13**, 1075 (1988).

[8] J. Mlynek, C. Tamm, E. Buhr, and N. C. Wong, Phys. Rev. Lett. **53**, 1814 (1984); C. Tamm, E. Buhr, and J. Mlynek, Phys. Rev. A **34**, 1977 (1986).

[9] M. E. Rose, *Elementary Theory of Angular Momentum* (Wiley, New York, 1957).

[10] $D^{(5/2)}_{i,j}(\alpha,\beta,\gamma)$ is the i,j component of the rotation operator $R(\alpha,\beta,\gamma)$.

[11] See, for example, R. M. Macfarlane and R. M. Shelby, in *Spectroscopy of Crystals Containing Rare Earth Ions,* edited by A. A. Kaplyanskii and R. M. Macfarlane (North-Holland, Amsterdam, 1987).

[12] The definition of α_m and ξ_m is the same as α_i and ξ_i in Ref. 2 except that the ranges of α_m and ξ_m are taken to be $0\le\alpha_m\le\pi/2$ and $-\pi/2\le\xi_m\le 3\pi/2$. The values of α_m ($m=\frac{5}{2},\frac{1}{2},-\frac{3}{2}$) (Table IV in Ref. 2) generally depend on the assignment of the quadrupole axes (X,Y,Z) and so are those of α_m and ξ_m. For convenience we take the assignments different from those in Ref. 2 (see Fig. 4). This results in the change of the values of α_m.

[13] See, for example, A. Abragam, *The Principles of Nuclear Magnetism* (Oxford University Press, London, 1961).

[14] T. Endo, T. Muramoto, and T. Hashi, Opt. Commun. **46**, 47 (1983).